

# Bond distortion effects and electric orders in spiral multiferroic magnets

Hong-Bo Chen, Yi Zhou and You-Quan Li

Zhejiang Institute of Modern Physics and Department of Physics,  
Zhejiang University, Hangzhou 310027, People's Republic of China

(Dated: November 11, 2018)

We study in this paper bond distortion effect on electric polarization in spiral multiferroic magnets based on cluster and chain models. The bond distortion break inversion symmetry and modify the  $d$ - $p$  hybridization. Consequently, it will affect electric polarization which can be divided into spin-current part and lattice-mediated part. The spin-current polarization can be written in terms of  $\vec{e}_{i,j} \times (\vec{e}_i \times \vec{e}_j)$  and the lattice-mediated polarization exists only when the M-O-M bond is distorted. The electric polarization for three-atom M-O-M and four-atom M-O<sub>2</sub>-M clusters is calculated. We also study possible electric ordering in three kinds of chains made of different clusters. We apply our theory to multiferroics cuprates and find that the results are in agreement with experimental observations.

## I. INTRODUCTION

Magnetoelectric multiferroics, where magnetic and electric ordering coexisting in a single compound, has attracted much interest in the last decades due to their potential for novel physics and technological applications<sup>1</sup>. However, the initial observations have shown that materials with coexisting ferroelectric and magnetic orders are rare in nature and the observed magnetoelectric coupling was rather weak<sup>2</sup>. Therefore, the search for new gigantic magnetoelectric multiferroic materials is a great challenge. As an important progress in multiferroics, Kimura *et al.*<sup>3</sup> found giant magnetoelectric effects in the perovskite manganite TbMnO<sub>3</sub> in 2003. The ferroelectric transition at  $T_c = 28$  K in TbMnO<sub>3</sub> was ascribed to the emergence of a nontrivial magnetic order, i.e., with a spiral spin structure<sup>4</sup>. This finding revived the interests in multiferroic behavior and lead to the discovery of a relatively large number of spin-driven multiferroic materials<sup>5-7</sup>.

One of the fundamental issues in multiferroic physics is to clarify the origin of the magnetoelectric coupling in such new materials. Currently, although several models have been proposed both microscopically<sup>8-17</sup> and phenomenologically<sup>18</sup>, the microscopic mechanism of the magnetoelectric coupling is still a controversial and unresolved topic. One of the most prevailing mechanisms is the spin-current model proposed by Katsura *et al.*<sup>8</sup> for helical magnets. They studied a three-atom M-O-M (M denotes a transition metal ion and O is for an oxygen ion) cluster where O locates in the inversion center of the cluster, say, the mid point between two M ions. They pointed out that spontaneous electric polarization in the spiral magnetic order arises from a distortion of electronic density even without ionic or atomic displacements. And the polarization can be expressed in the form

$$\vec{P} \propto \vec{e}_{i,j} \times (\vec{e}_i \times \vec{e}_j), \quad (1)$$

where  $\vec{e}_{i,j}$  denotes the bond direction connecting the two neighbor spin moments  $\vec{S}_i$  and  $\vec{S}_j$  along directions  $\vec{e}_i$  and  $\vec{e}_j$  on the sites  $i$  and  $j$  respectively. The electric

polarization is closely associated with the nonzero spin current  $\vec{S}_i \times \vec{S}_j$  between two neighboring noncollinear spins. Furthermore, Jia *et al.*<sup>9,10</sup> presented a more sophisticated calculation on the spin-current model with realistic considerations. Their results showed that the spin-current model is able to explain many experimental data at least semiquantitatively. On the other hand, Sergienko and Dagotto<sup>15</sup> argued that the ferroelectric polarization is closely related to the inverse Dzyaloshinskii-Moriya (DM) coupling which breaks inversion symmetry and obtained similar expression for electric polarization as in (1). Interestingly, the spin-orbit interaction plays a crucial role in both theories. The role of spin-orbit interaction was also confirmed by Mostovoy based on the phenomenological theory<sup>18</sup>. Experimentally, the spin-current mechanism was demonstrated directly by controlling the spin-helicity vector in TbMnO<sub>3</sub> with an external electric field<sup>19</sup>. The spin-current mechanism has also been applied to several other spiral multiferroic materials, such as DyMnO<sub>3</sub><sup>20</sup>, MnWO<sub>4</sub><sup>21</sup>, Ni<sub>3</sub>V<sub>2</sub>O<sub>8</sub><sup>22</sup>, CoCr<sub>2</sub>O<sub>4</sub><sup>23</sup>, LiCu<sub>2</sub>O<sub>2</sub><sup>24,25</sup> and LiCuVO<sub>4</sub><sup>26-29</sup>. Beside these successful applications, it should be noted that the magnitude of electric polarization is very sensitive to the location of Fermi energy in existing spin-current models. When the Fermi energy locates between two hybridized levels, which refers to “single hole” in Ref.<sup>8</sup>,  $P \propto V/\Delta$ , where  $V$  is the hybridization between transition metal  $d$ -orbitals and oxygen  $p$ -orbitals and  $\Delta$  is the energy difference between  $d$ -orbitals and  $p$ -orbitals. Whereas, when the Fermi energy locates outside two hybridized levels, which refers to “double hole” in Ref.<sup>8</sup>,  $P \propto (V/\Delta)^3$ , which is significantly different from “single hole” situation.

In real multiferroics, their fascinating properties are attributed to the competition among charge, spin, orbital, and lattice degrees of freedom. Actually, the bond-distortion is inevitably present in realistic transition metal oxides due to structure distortion<sup>30,31</sup>. Thus, the inversion symmetry breaks and the oxygen atom is away from the mid point between two M atoms. Therefore, the bond-distortion effects should be taken into account in the calculation for the electric polarization. In

existing spin-current model<sup>8–10</sup>, the bond-distortion effect is overlooked. As a result that we shall show in this paper, the calculated electric polarization is underestimated. A recent theoretical study on a toy model for the ferroelectricity of a two-dimensional cluster<sup>13</sup> suggests that the bond-bending may be important for the enhancement of the ferroelectricity due to orbital hybridization. On the other hand, Moskvina *et al.*<sup>32</sup> argued that the cluster model in Ref.<sup>8</sup> is oversimplified to account for LiCu<sub>2</sub>O<sub>2</sub> and LiCuVO<sub>4</sub> in which the realistic geometry configuration of the oxygen atoms was not considered. All of these facts motivate the present work to explore the effect of bond-distortion on the electric polarization in the spiral multiferroic magnets in the framework of spin-current model.

The organization of this paper is as follows. In Section II, we perform quantum chemistry analysis on relevant  $d$ -orbitals and construct cluster models with two M atoms and bridge oxygen atoms. Then we calculate lowest lying eigenstates for these cluster models. In Section III, we calculate the electric polarization for different clusters. In Section IV, we discuss three kinds of chain models formed by different clusters and possible ordering of electric polarization. In section V, we discuss the relation between lattice-driven polarization and magnetic-driven polarization and apply our theory to multiferroic copper oxides. Section VI is devoted to summary.

## II. CLUSTER MODELS

We begin with quantum chemistry consideration. As is well known, when the 3d transition metal atoms are placed in an octahedral crystal field, the five-fold degenerate  $d$  levels will split into  $e_g$  and  $t_{2g}$  levels. Incorporating the on-site spin-orbit interaction  $\lambda$ , the  $e_g$  orbitals will not be influenced but the  $t_{2g}$  manifold will further split into a doublet  $\Gamma_7$  and a quartet  $\Gamma_8$  (see Fig.1). For simplicity and following Katsura *et al.*<sup>8</sup>, we will adopt the following  $\Gamma_7$  states as the ground state manifold and drop the quartet,

$$\begin{aligned} |a\rangle &= \frac{1}{\sqrt{3}} (|d_{xy,\uparrow}\rangle + |d_{yz,\downarrow}\rangle + i|d_{zx,\downarrow}\rangle), \\ |b\rangle &= \frac{1}{\sqrt{3}} (|d_{xy,\downarrow}\rangle - |d_{yz,\uparrow}\rangle + i|d_{zx,\uparrow}\rangle), \end{aligned} \quad (2)$$

by assuming the spin-orbit coupling  $\lambda$  is the largest energy scale of the problem.

As in Ref.<sup>8</sup>, we further invoke the effective exchange interaction between  $\Gamma_7$  electrons and local magnetic moment governed by the following Hamiltonian,

$$H_U = -U \sum_j \vec{e}_j \cdot \vec{S}_j, \quad (3)$$

where  $\vec{e}_j = (\cos \phi_j \sin \theta_j, \sin \phi_j \sin \theta_j, \cos \theta_j)$  is the unit vector of the local magnetic moment from the transition metal atom M at  $j$ -th site,  $\vec{S}_j$  the total spin operator of the  $d$ -orbital electrons,  $U$  the effective exchange interaction which is of the order of Coulomb interaction

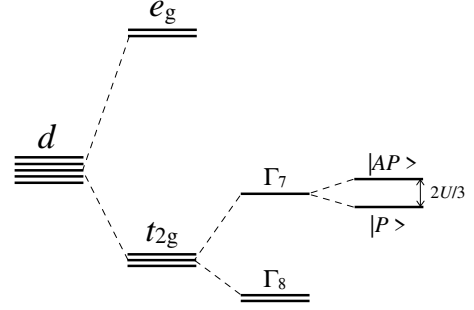


FIG. 1. Relevant electronic states at transition metal atoms. Five fold degenerate  $d$ -orbitals will split into two fold  $e_g$  and three fold  $t_{2g}$  levels. The spin-orbit interaction  $\lambda$  splits  $t_{2g}$  levels to a doublet  $\Gamma_7$  and a quartet  $\Gamma_8$ . In the presence of effective exchange  $U$  between  $\Gamma_7$  electrons and local magnetic moment,  $\Gamma_7$  will be further split into spin parallel state  $|P\rangle$  and antiparallel state  $|AP\rangle$ .

and Hund's coupling energy<sup>8–10</sup>. Then  $H_U$  will further split the  $\Gamma_7$  doublet into spin parallel state  $|P\rangle$  and antiparallel state  $|AP\rangle$ ,

$$|P_j\rangle = \sin \frac{\theta_j}{2} |a\rangle + e^{i\phi_j} \cos \frac{\theta_j}{2} |b\rangle, \quad (4a)$$

$$|AP_j\rangle = \cos \frac{\theta_j}{2} |a\rangle - e^{i\phi_j} \sin \frac{\theta_j}{2} |b\rangle, \quad (4b)$$

where  $|P_j\rangle$  and  $|AP_j\rangle$  indicate the spin state parallel and anti-parallel to the unit vector  $\vec{e}_j$ , and the corresponding eigenvalues are  $E_{|P_j\rangle} = -\frac{U}{3}$  and  $E_{|AP_j\rangle} = \frac{U}{3}$ , respectively. Note that we may further write  $|P_j\rangle$  and  $|AP_j\rangle$  in terms of  $t_{2g}$  states,

$$|P_j\rangle = \sum_{\mu\sigma} A_{(j)}^{\mu\sigma} |d_{\mu\sigma}^{(j)}\rangle, \quad (5a)$$

and

$$|AP_j\rangle = \sum_{\mu\sigma} B_{(j)}^{\mu\sigma} |d_{\mu\sigma}^{(j)}\rangle, \quad (5b)$$

where  $\mu = xy, yz, zx$ ,  $\sigma = \uparrow, \downarrow$ ,  $A_{(j)}^{\mu\sigma}$  and  $B_{(j)}^{\mu\sigma}$  are coefficients obtained from combining Eqs.(4) and (5) which depend on angles  $\theta_j$  and  $\phi_j$  (See Appendix A for details). Hereafter, we assume that  $\lambda$  and  $U$  are much larger than other relevant energy scales so that there is only one relevant state in each M atoms, say,  $|P\rangle$ . We also assume that there is a spiral magnetic order relating to the transition metal atoms.

Now we are in the position to construct cluster models by including bridge oxygen atoms between two M atoms. Taking the hole picture, we assume that the oxygen  $p$ -orbital has energy level  $E_p$  which is above  $E_{|P\rangle}$  with a difference  $\Delta$  as shown in Fig.2, i.e.  $E_p = E_{|P\rangle} + \Delta$ . The hybridization between spin parallel state  $|P\rangle$  and oxygen  $p$ -orbitals results in bonding and anti-bonding states with lower and higher energy respectively. In such a M-O-M cluster (see Fig.2), left and right bonding states will

further hybridize with each other and lead to two lowest energy levels  $E_1$  and  $E_2$ . When the Fermi energy  $E_F$  locates between  $E_1$  and  $E_2$ , it is called “single hole” in Ref.<sup>8</sup>. Whereas, it is called “double hole” when  $E_F$  is above  $E_2$  but below other levels.

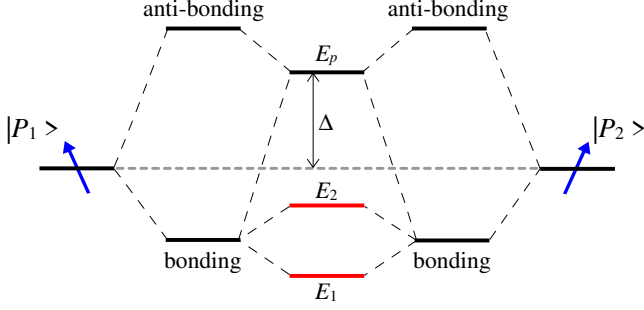


FIG. 2. Energy levels demonstration for a M-O-M cluster.

The hybridization between left and right bonding states will also lead to distorted electronic density and thereby possible electric polarization in such a M-O-M cluster. We may further consider more bridge oxygen atoms between two M atoms and derive similar electronic density distortion and electric polarization. We shall study three-atom M-O-M cluster and four-atom M-O<sub>2</sub>-M cluster in the remained part in this section and calculate electric polarization for different kinds of chains formed by three-atom or four-atom clusters in next section.

### A. Three-atom M-O-M cluster

Firstly we consider the three-atom M-O-M cluster model shown in Fig.3.  $M_1$  and  $M_2$  refer to two transition metal atoms and the intermediate oxygen atom (O) deviates from its centrosymmetric position on  $M_1$ - $M_2$  bond. To be simple, we assume that the three atoms of the cluster are restricted within the  $xy$ -plane, the  $M_1$ - $M_2$  bond is along the  $x$ -axis, and the lengths of two M-O bonds are equal to each other. Note that Katsura *et al.*<sup>8</sup> considered a centrosymmetric three-atom model in which the oxygen atom locates at the mid point between two M atoms.

Upon the above quantum chemistry analysis, we use the following Hamiltonian to describe the on-site energy for oxygen  $p$ -orbitals and spin parallel states,

$$H_\Delta = \sum_{j=1,2} E_{|P_j\rangle} c_{|P_j\rangle}^\dagger c_{|P_j\rangle} + \sum_{\mu,\sigma} (E_{|P\rangle} + \Delta) p_{\mu,\sigma}^\dagger p_{\mu,\sigma}, \quad (6)$$

where  $p_{\mu,\sigma}$ , ( $\mu = x, y, z$ ) are annihilation operators for oxygen  $p$ -electrons,  $\sigma$  is spin index,  $c_{|P_j\rangle}$  is the annihilation operator for spin parallel state at site  $j$ .

The hybridization between  $p$ -orbitals and spin parallel states is governed by the hopping Hamiltonian,

$$H_t = H_t^{1-m} + H_t^{2-m} + \text{H.c.}, \quad (7)$$

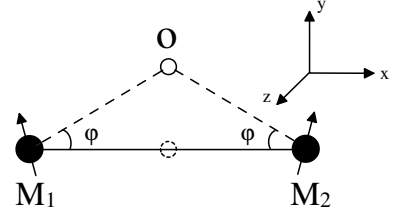


FIG. 3. Three atom M-O-M cluster model.  $M_1$  and  $M_2$  denote two transition metal ions with noncollinear magnetic moments. O represents a bridge oxygen atom which deviates from its centrosymmetric position (denoted by dash circle) with a bond-bending angle  $\varphi$ . The arrows on  $M_1$  and  $M_2$  indicate the spin direction. The three atoms of the cluster are assumed lying in the  $xy$  plane.

where  $H_t^{1-m}$  and  $H_t^{2-m}$  indicate the hopping processes between the oxygen atom and  $M_1$  and  $M_2$  respectively. We then write down  $H_t^{1-m}$  and  $H_t^{2-m}$  in terms of non-vanishing hopping integrals explicitly,

$$H_t^{1-m} = \sum_{\sigma} \left( V_1 p_{x,\sigma}^\dagger d_{xy,\sigma}^{(1)} + V_2 p_{y,\sigma}^\dagger d_{xy,\sigma}^{(1)} + V_3 p_{z,\sigma}^\dagger d_{zx,\sigma}^{(1)} + V_4 p_{z,\sigma}^\dagger d_{yz,\sigma}^{(1)} \right), \quad (8)$$

$$H_t^{2-m} = \sum_{\sigma} \left( V_1 p_{x,\sigma}^\dagger d_{xy,\sigma}^{(2)} - V_2 p_{y,\sigma}^\dagger d_{xy,\sigma}^{(2)} - V_3 p_{z,\sigma}^\dagger d_{zx,\sigma}^{(2)} + V_4 p_{z,\sigma}^\dagger d_{yz,\sigma}^{(2)} \right), \quad (9)$$

where  $d_{\mu,\sigma}^{(j)}$  ( $\mu = xy, yz, zx$ ) are annihilation operators for  $d$  electrons of the transition metal atoms. The superscript  $j = 1, 2$  in  $d_{\mu,\sigma}^{(j)}$  denote the site of magnetic transition metal atoms as shown in Fig.3. The integrals  $V_n$  ( $n = 1, 2, 3, 4$ ) between  $d$  and  $p$  orbitals are given according to Slater-Koster's rules<sup>33</sup> as follows,

$$\begin{aligned} V_1 &= \sin \varphi \left( \sqrt{3} \cos^2 \varphi t_{pd\sigma} + (1 - 2 \cos^2 \varphi) t_{pd\pi} \right), \\ V_2 &= \cos \varphi \left( \sqrt{3} \sin^2 \varphi t_{pd\sigma} + (1 - 2 \sin^2 \varphi) t_{pd\pi} \right), \\ V_3 &= \cos \varphi t_{pd\pi}, \\ V_4 &= \sin \varphi t_{pd\pi}. \end{aligned} \quad (10)$$

Here  $\varphi$  is the angle between  $M_1$ - $M_2$  bond (i.e., along  $x$ -axis) and  $M_{1(2)}$ -O bond, as shown in Fig. 3.  $t_{pd\sigma}$  and  $t_{pd\pi}$  are hybridization integrals corresponding to  $\sigma$  and  $\pi$  bonding between  $p$  and  $d$  orbitals respectively. In contrast to the hopping Hamiltonian derived by Katsura *et al.* in Ref.<sup>8</sup> where only  $t_{pd\pi}$  is present due to inversion symmetry, there are four relevant and independent hopping integrals  $V_n, n = 1, 2, 3, 4$ . Because more active orbitals are involved in our model due to the bond-distortion, such as  $p_x$  and  $d_{yz}$  orbitals. Thus, the Hilbert space in the present model is enlarged. The basis of the our cluster system contains  $|P_j\rangle$ , ( $j = 1, 2$ ) and  $p_{\mu,\sigma}$  ( $\mu = x, y, z, \sigma = \uparrow, \downarrow$ ) and an eigenstate is a linear combination of these states. We can easily recover centrosym-

metric cluster model in Ref.<sup>8</sup> by setting  $\varphi = 0$ , which leads to  $V_1 = V_4 = 0$  and  $V_2 = V_3$ .

We proceed to calculate the eigenstates of the system by assuming  $V \ll \Delta$  and treating  $H_t$  as a perturbation to  $H_\Delta$ . To the second order perturbation<sup>34</sup>, the two lowest lying states are given by energy levels

$$E_{1(2)} = 2(C \mp |B|), \quad (11)$$

with corresponding eigenvectors  $|1\rangle$  and  $|2\rangle$  given in Appendix B, where the parameters  $C$  and  $B$  are as follows,

$$C = -\frac{V_1^2 + V_2^2 + V_3^2 + V_4^2}{3\Delta}, \quad (12)$$

$$B = A_1\alpha + A_2\beta,$$

with

$$A_1 = -\frac{V_1^2 - V_2^2 - V_3^2 + V_4^2}{3\Delta},$$

$$A_2 = \frac{2V_3V_4}{3\Delta}, \quad (13)$$

and

$$\alpha = \sin \frac{\theta_1}{2} \sin \frac{\theta_2}{2} + \cos \frac{\theta_1}{2} \cos \frac{\theta_2}{2} e^{-i(\phi_1 - \phi_2)},$$

$$\beta = i[\sin \frac{\theta_1}{2} \sin \frac{\theta_2}{2} - \cos \frac{\theta_1}{2} \cos \frac{\theta_2}{2} e^{-i(\phi_1 - \phi_2)}]. \quad (14)$$

The angles  $(\theta_1, \phi_1)$  and  $(\theta_2, \phi_2)$  specify the direction of local magnetic moments in transition metal atom  $M_1$  and  $M_2$  respectively. For a centrosymmetric cluster with  $\varphi = 0$ , we have  $A_2 = 0$  and  $C = -A_1$ .

### B. Four-atom M-O<sub>2</sub>-M cluster

Secondly, we consider the four-atom M-O<sub>2</sub>-M cluster illustrated in Fig.4. In this situation, there are two oxygen atoms symmetrically deviated away from the  $M_1$ - $M_2$  bond with a bond-distortion angle  $\varphi$ . Here, we also assume that the atoms of the cluster are restricted within the  $xy$  plane and the  $M_1$ - $M_2$  bond is along the  $x$ -axis for convenience.

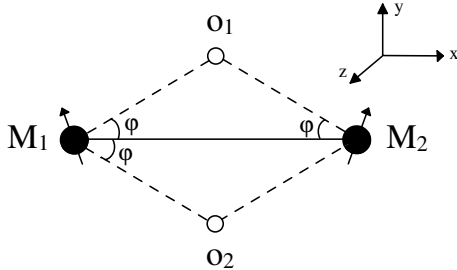


FIG. 4. Four-atom  $M_1$ - $O_{1(2)}$ - $M_2$  cluster. Two bridge oxygen atoms  $O_1$  and  $O_2$  symmetrically deviates from  $M_1$ - $M_2$  bond with a bond-distortion angle  $\varphi$ . The arrows on  $M_1$  and  $M_2$  indicate the directions of spins. The four atoms of this cluster lie within the  $xy$  plane and  $M_1$ - $M_2$  bond lies along the  $x$ -axis.

The on-site energy in Eq.(6) is then modified as

$$H_\Delta = \sum_{j=1,2} E_{|P\rangle} c_{|Pj\rangle}^\dagger c_{|Pj\rangle} + \sum_{i,\mu,\sigma} (E_{|P\rangle} + \Delta) p_{\mu,\sigma}^{(i)\dagger} p_{\mu,\sigma}^{(i)}, \quad (15)$$

where the superscript  $i = 1, 2$  in  $p_{\mu,\sigma}^{(i)}$ , ( $\mu = x, y, z$ ) denote the site number for oxygen atoms  $O_1$  and  $O_2$  shown in Fig.4. Note that we assume that  $p$  orbitals in the two oxygen atoms  $O_1$  and  $O_2$  has the same energy levels, say,  $E_{p_1} = E_{p_2} = E_{|P\rangle} + \Delta$ , due to the symmetric deviation of two oxygen atoms.

Accordingly, we shall replace hopping terms  $H_t^{1-m}$  and  $H_t^{2-m}$  in Eq. (8) and Eq. (9) by

$$H_t^{1-m} = \sum_{\sigma} \left( V_1 p_{x,\sigma}^{(1)\dagger} d_{xy,\sigma}^{(1)} + V_2 p_{y,\sigma}^{(1)\dagger} d_{xy,\sigma}^{(1)} + V_3 p_{z,\sigma}^{(1)\dagger} d_{zx,\sigma}^{(1)} \right. \\ \left. + V_4 p_{z,\sigma}^{(1)\dagger} d_{yz,\sigma}^{(1)} - V_1 p_{x,\sigma}^{(2)\dagger} d_{xy,\sigma}^{(1)} + V_2 p_{y,\sigma}^{(2)\dagger} d_{xy,\sigma}^{(1)} \right. \\ \left. + V_3 p_{z,\sigma}^{(2)\dagger} d_{zx,\sigma}^{(1)} - V_4 p_{z,\sigma}^{(2)\dagger} d_{yz,\sigma}^{(1)} \right), \quad (16)$$

and

$$H_t^{2-m} = \sum_{\sigma} \left( V_1 p_{x,\sigma}^{(1)\dagger} d_{xy,\sigma}^{(2)} - V_2 p_{y,\sigma}^{(1)\dagger} d_{xy,\sigma}^{(2)} - V_3 p_{z,\sigma}^{(1)\dagger} d_{zx,\sigma}^{(2)} \right. \\ \left. + V_4 p_{z,\sigma}^{(1)\dagger} d_{yz,\sigma}^{(2)} - V_1 p_{x,\sigma}^{(2)\dagger} d_{xy,\sigma}^{(2)} - V_2 p_{y,\sigma}^{(2)\dagger} d_{xy,\sigma}^{(2)} \right. \\ \left. - V_3 p_{z,\sigma}^{(2)\dagger} d_{zx,\sigma}^{(2)} - V_4 p_{z,\sigma}^{(2)\dagger} d_{yz,\sigma}^{(2)} \right), \quad (17)$$

respectively, where  $V_n$  ( $n = 1, 2, 3, 4$ ) are the same hybridization integrals defined in Eqs. (10). As shown in the previous subsection, due to the oxygen atoms displacements, there are more active orbitals involved. Relevant states in such a four-atom cluster include  $|P_j\rangle$ ,  $|AP_j\rangle$  and  $p_{\mu,\sigma}^{(i)}$ , where  $i, j = 1, 2$ ,  $\mu = x, y, z$ ,  $\sigma = \uparrow, \downarrow$ .

In the similar way as the three-atom cluster, the two lowest lying states of the four-atom cluster can be obtained with energy levels,

$$E_{1(2)} = 2(C \mp |A_1\alpha|), \quad (18)$$

and corresponding eigenvectors  $|1\rangle$  and  $|2\rangle$  given in Appendix C, where the parameters  $C$ ,  $A_1$  and  $\alpha$  are those given in Eqs. (12), (13) and (14).

### III. ELECTRIC POLARIZATION IN CLUSTERS

We shall calculate electric polarizations  $\vec{P} = \langle e\vec{r} \rangle$  for three-atom M-O-M clusters or four-atom M-O<sub>2</sub>-M clusters using the states  $|1\rangle$  and  $|2\rangle$  obtained from cluster models in previous section. The position of Fermi energy  $E_F$  is crucial to determine the expectation value  $\vec{P}$ , which is given by

$$\vec{P} = n_F(E_1 - E_F) \frac{\langle 1 | e\vec{r} | 1 \rangle}{\langle 1 | 1 \rangle} + n_F(E_2 - E_F) \frac{\langle 2 | e\vec{r} | 2 \rangle}{\langle 2 | 2 \rangle}, \quad (19)$$

where  $n_F(E) = \frac{1}{1 + e^{\beta E}}$  is the Fermi function. At low temperature, one may replace  $n_F(E)$  by  $\theta(-E)$ . In the

case of single-hole, say,  $E_1 < E_F < E_2$ , only the lowest state  $|1\rangle$  contributes to electric polarization. While in the double-hole situation,  $E_F > E_2$ , both state  $|1\rangle$  and  $|2\rangle$  are active<sup>8</sup>.

According to the expression of  $|1\rangle$  and  $|2\rangle$  given in Appendix B and Appendix C, the electric polarization  $\vec{P}$  can be written in terms of the overlap dipole matrix elements  $I_{\mu,\nu}^\alpha(\vec{a})$  given as follows,

$$I_{\mu,\nu}^\alpha(\vec{a}) = e \langle d_\mu(\vec{r}) | \alpha | p_\nu(\vec{r} + \vec{a}) \rangle, \quad (20)$$

where  $\vec{a}$  is the displacement from a transition metal atom M to one of its neighboring oxygen atoms O,  $\alpha = x, y, z$  is one of the three components of  $\vec{r}$ ,  $\mu = xy, yz, zx$  denotes three  $t_{2g}$  orbitals and  $\nu = x, y, z$  denotes three oxygen  $p$ -orbitals. We calculate  $I_{\mu,\nu}^\alpha(\vec{a})$  in Appendix D and study the configurations of electric polarization in the following subsections.

We find that the electric polarization consists of two parts. The first part can be written in terms of  $\vec{e}_j \times \vec{e}_{j+1}$ , which is called “spin-current polarization”. The second part depends on the bond bending angle and distortion configuration, which is called “lattice-mediated polarization”.

### A. Three-atom M-O-M cluster

For a three-atom M-O-M cluster, both spin-current polarization and lattice-mediated polarization contribute to the electric polarization. However, they may play different roles in different situations. We shall discuss single-hole and double-hole situations respectively.

For *single-hole situation* when  $E_1 < E_F < E_2$ , only the lowest state  $|1\rangle$  contributes to electric polarization. The induced electric polarization  $\vec{P}_{j,j+1}$  at each element cluster connecting  $j$  and  $j+1$ -th transition metal atoms can be calculated with the help of Eq. (B1). The resulting polarization with three components reads,

$$\begin{aligned} P_{j,j+1}^x &= 0, \\ P_{j,j+1}^y &= \frac{1}{3} \frac{I_1^y A_1 + I_2^y A_2}{\Delta |B_{j,j+1}|} (\vec{e}_{j,j+1} \times (\vec{e}_j \times \vec{e}_{j+1}))|_y \\ &\quad - \frac{2}{3} \frac{I_3^y}{\Delta} - \frac{2}{3} \frac{I_2^y A_1 |\alpha_{j,j+1}|^2 + I_1^y A_2 |\beta_{j,j+1}|^2}{\Delta |B_{j,j+1}|}, \\ P_{j,j+1}^z &= \frac{1}{3} \frac{I_4^z A_1}{\Delta |B_{j,j+1}|} (\vec{e}_{j,j+1} \times (\vec{e}_j \times \vec{e}_{j+1}))|_z \\ &\quad + \frac{1}{3} \frac{I_4^z A_2}{\Delta |B_{j,j+1}|} (\sin \theta_j \cos \theta_{j+1} \sin \phi_j \\ &\quad + \cos \theta_j \sin \theta_{j+1} \sin \phi_{j+1}), \quad (21) \end{aligned}$$

where  $B_{j,j+1} = A_1 \alpha_{j,j+1} + A_2 \beta_{j,j+1}$ , and  $\alpha_{j,j+1}$  and

$\beta_{j,j+1}$  are given as follows,

$$\begin{aligned} \alpha_{j,j+1} &= \sin \frac{\theta_j}{2} \sin \frac{\theta_{j+1}}{2} + \cos \frac{\theta_j}{2} \cos \frac{\theta_{j+1}}{2} e^{-i(\phi_j - \phi_{j+1})}, \\ \beta_{j,j+1} &= i(\sin \frac{\theta_j}{2} \sin \frac{\theta_{j+1}}{2} - \cos \frac{\theta_j}{2} \cos \frac{\theta_{j+1}}{2} e^{-i(\phi_j - \phi_{j+1})}), \end{aligned} \quad (22)$$

by replacing  $\phi_1$  and  $\phi_2$  in Eq.(14) by  $\phi_j$  and  $\phi_{j+1}$  respectively. And other parameters are defined as

$$\begin{aligned} I_1^y &= V_3 I_{yz,z}^y + V_4 I_{zx,z}^y, \\ I_2^y &= -V_1 I_{xy,x}^y + V_2 I_{xy,y}^y + V_3 I_{zx,z}^y - V_4 I_{yz,z}^y, \\ I_3^y &= V_1 I_{xy,x}^y + V_2 I_{xy,y}^y + V_3 I_{zx,z}^y + V_4 I_{yz,z}^y, \\ I_4^z &= V_2 I_{yz,y}^z + V_4 I_{xy,z}^z - V_1 I_{yz,x}^z. \end{aligned} \quad (23)$$

Each component in the electric polarization  $\vec{P}_{j,j+1}$  contains two parts, one part can be written in terms of  $\vec{e}_j \times \vec{e}_{j+1}$  which has been predicted in Ref.<sup>8</sup>, the other part is related to the bond distortion and depends on the bending angle  $\varphi$ . We denote the second part subject to bond distortion as “lattice-mediated”, to distinguish it from the “spin-current” polarization in the first part. Note that, both lattice-mediated contribution and spin-current contribution are of the order of  $V/\Delta$  and comparable to each other when  $\varphi$  is large enough. To derive  $P_{j,j+1}^x$ , we use the condition that the two M atoms locate mirror-symmetrically about the  $yz$  plane across the oxygen atom and the  $\Gamma_7$  manifold in Eq.(2) which keeps unchanged under the mirror operation  $x \rightarrow -x$ .

For *double-hole situation* when  $E_F > E_2$ , two lowest states  $|1\rangle$  and  $|2\rangle$  are involved. Using Eq.(19) and Eqs.(B1) (B2), we can easily calculate the electric polarization  $\vec{P}_{j,j+1}$ , which results in

$$\begin{aligned} P_{j,j+1}^x &= 0, \\ P_{j,j+1}^y &= -\frac{2}{3} \frac{I_1^y A_1 + I_2^y A_2}{\Delta^2} (\vec{e}_{j,j+1} \times (\vec{e}_j \times \vec{e}_{j+1}))|_y \\ &\quad - \frac{4}{3} \frac{I_3^y}{\Delta} \left(1 + \frac{C}{\Delta}\right) + \frac{4}{3} \frac{I_2^y A_1 |\alpha_{j,j+1}|^2 + I_1^y A_2 |\beta_{j,j+1}|^2}{\Delta^2}, \\ P_{j,j+1}^z &= -\frac{2}{3} \frac{I_4^z A_1}{\Delta^2} (\vec{e}_{j,j+1} \times (\vec{e}_j \times \vec{e}_{j+1}))|_z \\ &\quad - \frac{2}{3} \frac{I_4^z A_2}{\Delta^2} (\sin \theta_j \cos \theta_{j+1} \sin \phi_j \\ &\quad + \cos \theta_j \sin \theta_{j+1} \sin \phi_{j+1}). \end{aligned} \quad (24)$$

To derive  $\vec{P}_{j,j+1}$ , we have made the approximation  $\langle 1|1 \rangle^{-1} \approx 1 + (C - |B|)/\Delta$  and  $\langle 2|2 \rangle^{-1} \approx 1 + (C + |B|)/\Delta$ . Similar to the single-hole situation, the electric polarization can be divided into two parts, the lattice mediated contribution and the spin-current contribution too. However, it is different from the single-hole situation that the spin-current contribution is of the order of  $(V/\Delta)^3$  while the lattice mediated part is of the order of  $V/\Delta$ . Because the electric polarization contains two parts from states  $|1\rangle$  and  $|2\rangle$  respectively which tend to cancel each other<sup>8</sup>. So the lattice mediated contribution will dominate over spin-current contribution when  $\varphi$  is large enough.

### B. Four-atom M-O<sub>2</sub>-M cluster

For a four-atom M-O<sub>2</sub>-M cluster, only the spin-current polarization contributes to the electric polarization while lattice-mediated polarization vanishes. Using the results in Appendix C, one can calculate electric polarization straightforward.

For *single-hole situation*, one obtains that

$$\begin{aligned} P_{j,j+1}^x &= 0, \\ P_{j,j+1}^y &= \frac{2 I_1^y A_1}{3 \Delta |A_1|} \frac{(\vec{e}_{j,j+1} \times (\vec{e}_j \times \vec{e}_{j+1}))}{|\alpha_{j,j+1}|} \Big|_y, \\ P_{j,j+1}^z &= \frac{2 I_4^z A_1}{3 \Delta |A_1|} \frac{(\vec{e}_{j,j+1} \times (\vec{e}_j \times \vec{e}_{j+1}))}{|\alpha_{j,j+1}|} \Big|_z, \end{aligned} \quad (25)$$

where  $\alpha_{j,j+1}$  is given in Eq.(22).

For *double-hole situation*, one obtains that

$$\begin{aligned} P_{j,j+1}^x &= 0, \\ P_{j,j+1}^y &= -\frac{8 I_1^y A_1}{3 \Delta^2} (\vec{e}_{j,j+1} \times (\vec{e}_j \times \vec{e}_{j+1})) \Big|_y, \\ P_{j,j+1}^z &= -\frac{8 I_4^z A_1}{3 \Delta^2} (\vec{e}_{j,j+1} \times (\vec{e}_j \times \vec{e}_{j+1})) \Big|_z. \end{aligned} \quad (26)$$

One sees that lattice-mediated contribution to the electric polarization is canceled due to the reflection symmetry between two oxygen atoms in such a M-O<sub>1(2)</sub>-M cluster.

## IV. CHAIN MODELS AND ELECTRIC ORDERS

We go further to investigate different chains formed by three-atom M-O-M clusters or four-atom M-O<sub>2</sub>-M clusters and study possible electric orders in such chains. Since most multiferroics are insulators, relevant electrons are localized within clusters, we may neglect electron hopping between clusters and use relevant local states  $|1\rangle$  and  $|2\rangle$  obtained from cluster models in previous section to calculate the electric polarization  $\vec{P}$  within each cluster.

### A. Uniform bending M-O-M chain

Firstly, we consider the uniform bond-distortion chain model shown in Fig.5. In this case, all the bridge oxygen atoms deviate from the spin chain formed by transition metal atoms in the same direction and with the same bond-bending angle  $\varphi$ . This type of bond-distortion may be ascribed to the DM interaction relating to spiral spin ordering, where the spin-helicity vector has the same sign for all pairs of neighbouring spins in case of transverse-spiral ordering, the DM coupling pushes negative oxygen ions in the same direction<sup>5</sup>.

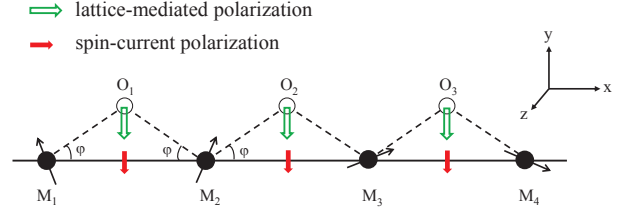


FIG. 5. (Color online) A sketch of the uniform bending M-O-M chain. All the bridge oxygen atoms deviate from the transition metal atoms chain in the same direction and lie within the  $xy$ -plane. And the spin-spiral plane is  $xy$ -plane. The spin-current and lattice-mediated polarization are denoted by red and green arrows, respectively.

It is easy to see that ferroelectric order will form in this kind of chains. To illustrate it, we assume all the magnetic moment from transition metal ions lie in  $xy$ -plane and are spiral ordered in the same plane as shown in Fig.5. In this case,  $P_{j,j+1}^x = P_{j,j+1}^z = 0$ , and  $P_{j,j+1}^y$  does not depend on site index  $j$ .

For single-hole,

$$\begin{aligned} P_{j,j+1}^y &= \frac{1}{3} \frac{I_1^y A_1 + I_2^y A_2}{\Delta} \frac{\sin(\Delta\phi)}{|A_1 \cos \frac{\Delta\phi}{2} - A_2 \sin \frac{\Delta\phi}{2}|} \\ &\quad - \frac{2}{3} \frac{I_3^y}{\Delta} - \frac{2}{3} \frac{I_2^y A_1}{\Delta} \frac{|\cos \frac{\Delta\phi}{2}|^2 + I_1^y A_2 |\sin \frac{\Delta\phi}{2}|^2}{|A_1 \cos \frac{\Delta\phi}{2} - A_2 \sin \frac{\Delta\phi}{2}|}, \end{aligned} \quad (27)$$

while for double-hole,

$$\begin{aligned} P_{j,j+1}^y &= -\frac{2}{3} \frac{I_1^y A_1 + I_2^y A_2}{\Delta^2} \sin(\Delta\phi) - \frac{4}{3} \frac{I_3^y}{\Delta} \left(1 + \frac{C}{\Delta}\right) \\ &\quad + \frac{4}{3} \frac{I_2^y A_1}{\Delta^2} \frac{|\cos \frac{\Delta\phi}{2}|^2 + I_1^y A_2 |\sin \frac{\Delta\phi}{2}|^2}{\Delta^2}, \end{aligned} \quad (28)$$

with  $\Delta\phi = \phi_j - \phi_{j+1}$ .

### B. Staggered bending M-O-M chain

There also exist some materials with staggered bending M-O-M chains as shown in Fig.6. For instance, the Mn-O-Mn-O-Mn bonding along  $\langle 110 \rangle$  direction forms a zigzag chain due to alternative rotation and tilt of the MnO<sub>6</sub> octahedra in some perovskite rare earth manganese oxides RMnO<sub>3</sub><sup>31</sup>.

In this case, spin-current polarization and lattice-mediated polarization may form different orders. To illustrate it, we still assume all the magnetic moment from transition metal ions lie in  $xy$ -plane and are spiral ordered as shown in Fig.6. In this case,  $P_{j,j+1}^x = P_{j,j+1}^z = 0$ .  $P_{j,j+1}^y$  contains two parts, spin-current polarization  $P_{j,j+1}^{sc,y}$  and lattice-mediated polarization  $P_{j,j+1}^{lm,y}$ ,

$$P_{j,j+1}^y = P_{j,j+1}^{sc,y} + P_{j,j+1}^{lm,y}. \quad (29)$$

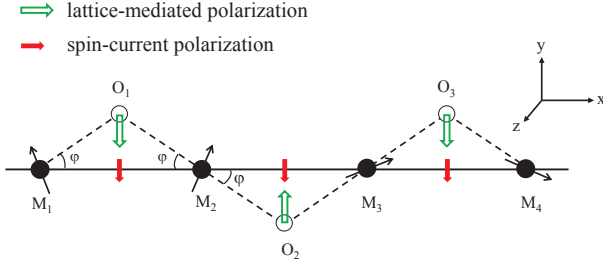


FIG. 6. (Color online) A sketch of the staggered M-O-M chain. The neighbor oxygen atoms of a given magnetic metal atom displace toward opposite directions. The spin-current polarization is uniform in each M-O-M cluster (red arrows), while lattice-mediated polarization is staggered (green arrows).

For single-hole,

$$P_{j,j+1}^{sc,y} = \frac{1}{3} \frac{I_1^y A_1 + I_2^y A_2}{\Delta} \frac{\sin(\Delta\phi)}{\left| A_1 \cos \frac{\Delta\phi}{2} + (-1)^j A_2 \sin \frac{\Delta\phi}{2} \right|},$$

$$P_{j,j+1}^{lm,y} = (-1)^j \frac{2}{3} \frac{I_3^y}{\Delta} + (-1)^j \frac{2}{3} \frac{I_2^y A_1 \left| \cos \frac{\Delta\phi}{2} \right|^2 + I_1^y A_2 \left| \sin \frac{\Delta\phi}{2} \right|^2}{\Delta \left| A_1 \cos \frac{\Delta\phi}{2} + (-1)^j A_2 \sin \frac{\Delta\phi}{2} \right|}. \quad (30)$$

while for double-hole,

$$P_{j,j+1}^{sc,y} = -\frac{2}{3} \frac{I_1^y A_1 + I_2^y A_2}{\Delta^2} \sin(\Delta\phi),$$

$$P_{j,j+1}^{lm,y} = (-1)^j \frac{4}{3} \frac{I_3^y}{\Delta} \left( 1 + \frac{C}{\Delta} \right) + (-1)^{j+1} \frac{4}{3} \frac{I_2^y A_1 \left| \cos \frac{\Delta\phi}{2} \right|^2 + I_1^y A_2 \left| \sin \frac{\Delta\phi}{2} \right|^2}{\Delta^2}. \quad (31)$$

So that spin-current polarization is uniform and forms ferroelectric order while lattice-mediated polarization is staggered and forms antiferroelectric order. The total electric polarization is “*ferrielectric ordered*”.

### C. Symmetric M-O<sub>2</sub>-M chain

Finally, we consider a symmetric M-O<sub>2</sub>-M chain shown in Fig.7, which is made of four-atom M-O<sub>2</sub>-M clusters. Such symmetric M-O<sub>2</sub>-M chains exist in two prominent examples of multiferroic compound, namely, LiCu<sub>2</sub>O<sub>2</sub><sup>24,25</sup> and LiCuVO<sub>4</sub><sup>26</sup>, which crystallize as one-dimensional chains of the edge-sharing CuO<sub>4</sub> plaquettes.

In this kind of chains, lattice-mediated polarization vanishes and spin-current polarization may form ferroelectric order. Assuming all the magnetic moment from

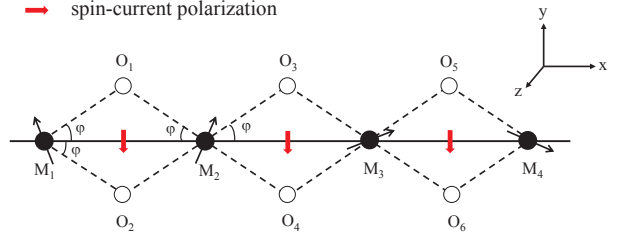


FIG. 7. (Color online) A schematic edge-shared MO<sub>2</sub> chain. The bridge oxygen atoms are symmetrically located beside the two sides of the magnetic metal atoms chain. In this case, the lattice-mediated contribution of the electric polarization is exactly canceled. The nonvanish part of the polarization arise from the spin current, indicated by red arrows.

transition metal ions lie in *xy*-plane and are spiral ordered as shown in Fig.7, we obtain  $P_{j,j+1}^x = P_{j,j+1}^z = 0$  and

$$P_{j,j+1}^y = \frac{2}{3} \frac{I_1^y A_1}{\Delta |A_1|} \frac{\sin(\Delta\phi)}{\left| \cos \frac{\Delta\phi}{2} \right|}, \quad (32)$$

in single-hole situation and

$$P_{j,j+1}^y = -\frac{8}{3} \frac{I_1^y A_1}{\Delta^2} \sin(\Delta\phi), \quad (33)$$

in double-hole situation.

## V. DISCUSSIONS

In this section, we shall discuss the relation between magnetism-driven electric polarization and lattice-driven electric polarization, and then apply our theory to multiferroic copper oxides.

*Lattice-driven electric polarization:* As shown in Fig.5, the negatively charged oxygens coherently displace away from the magnetic chain formed by M ions. This shift will generate a net *lattice-driven* electric polarization  $P^{ld}$  directing from the oxygen ions to the M ions chain. The polarization  $P^{ld}$  can be evaluated as long as the *p-d* hybridizations  $t_{pd\sigma}$  and  $t_{pd\pi}$  and the geometry of the lattice are specified. We shall compare this lattice-driven electric polarization ( $P^{ld}$ ) with the two parts of magnetism-driven electric polarization studied in this paper, say, lattice-mediated polarization ( $P^{lm}$ ) and spin-current polarization ( $P^{sc}$ ). To do this, we restrict ourselves to the double-hole situation and choose the following parameters,  $t_{pd\sigma}/t_{pd\pi} = -2$ ,<sup>35</sup>  $\Delta = 2\text{eV}$ ,  $\sin(\Delta\phi) = \sin(0.28\pi)$ <sup>10,12,14</sup> and the lattice constant  $a = 5\text{\AA}$ . The results are shown in Fig.8 where electric polarizations are plotted as functions of bond-bending angle  $\varphi$ . For a typical  $\varphi$ ,  $P^{ld} \sim 10^2 \mu\text{C}/\text{m}^2$ , while  $P^{lm} \sim 10^2 \mu\text{C}/\text{m}^2$  and  $P^{sc} \sim 10 \mu\text{C}/\text{m}^2$ . The lattice-mediated polarization keeps in parallel with the lattice-driven polarization for any bond-bending angle  $\varphi$  while the spin current polarization may varies with  $\varphi$  and be in parallel or anti-parallel to the lattice-driven polarization. Moreover, the



spin current polarization depends on spin configuration and can be neither parallel nor anti-parallel to lattice-driven polarization. Upon these observations, we conclude that lattice-driven polarization is cooperative with lattice-mediated polarization while spin current polarization may be either competitive or cooperative, depending on the spin configuration and the bond-bending angle.

Note that lattice-driven polarization  $P^{ld}$  in Fig.8(a) is overestimated since we chose the maximum electric polarization in all the possible valences for magnetic transition metal and oxygen ions. It is also worth noting that although  $P^{ld}$  and  $P^{lm}$  dominate over  $P^{sc}$  at finite  $\varphi$  in uniform bending chains as shown in Fig.8,  $P^{sc}$  will be dominating at small  $\varphi$  or in symmetric M-O<sub>2</sub>-M chains.

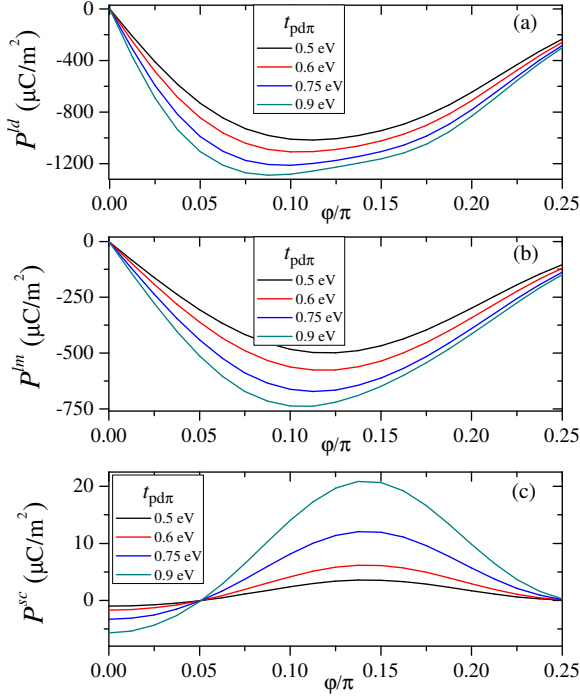


FIG. 8. (Color online) The  $\varphi$ -dependence of electric polarizations in uniform bending M-O-M chains (see Fig.5). (a) Lattice-driven electric polarization. (b) Lattice-mediated polarization. (c) Spin-current polarization.

*Multiferroic copper oxides:* Then we shall apply our theory to several copper oxides, including LiCuVO<sub>4</sub>, LiCu<sub>2</sub>O<sub>2</sub> and NaCu<sub>2</sub>O<sub>2</sub>, where magnetic copper ions Cu<sup>2+</sup> and oxygen ions O<sup>2-</sup> form symmetric M-O<sub>2</sub>-M chain as shown in Fig.7.

There are two prominent compounds which can be described symmetric M-O<sub>2</sub>-M chains, LiCu<sub>2</sub>O<sub>2</sub> and LiCuVO<sub>4</sub>. Both of them are characterized by edge-sharing CuO<sub>4</sub> plaquettes, forming spiral spin orders and emerging electric polarization at low temperature. The electric polarization in these two compounds is relatively weak comparing with manganites,  $\sim 10 \mu\text{C}/\text{m}^2$ , and shows strong anisotropy. There is another interesting material NaCu<sub>2</sub>O<sub>2</sub>, which is isostructural to LiCu<sub>2</sub>O<sub>2</sub>

while Li is substituted by Na. Although NaCu<sub>2</sub>O<sub>2</sub> also exhibits helical magnetic order at low temperature<sup>36–38</sup>, no electric polarization has been observed in it within the experimental sensitivity ( $< 0.3 \mu\text{C}/\text{m}^2$ )<sup>39,40</sup>. We shall apply our theory to these prototypical compounds and address the issue of “missing multiferroicity” in NaCu<sub>2</sub>O<sub>2</sub> in the rest of this section.

As mentioned in Section III B, the lattice-mediated contribution is exactly cancelled in a symmetric M-O<sub>2</sub>-M cluster, and the electric polarization comes from the spin current only. In contrast to widely used isotropic form of Eq.(1), the spin current form of electric polarization in the symmetric M-O<sub>2</sub>-M cluster is anisotropic in general, which is in accord with the experimental findings<sup>24,25,27,28</sup> and density functional calculations<sup>41</sup>. The magnitude of the electric polarization depends on the bond-bending angle  $\varphi$  and vanishes at  $\varphi = \pi/4$ . Note that the spin current form will recover isotropic in the absence of bond distortion, say,  $\varphi = 0$ .

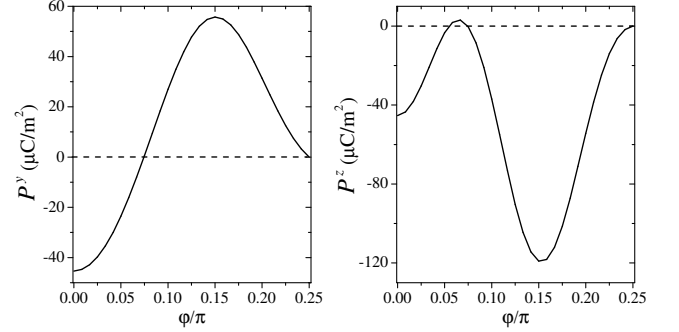


FIG. 9. The  $\varphi$ -dependence of  $y$ - and  $z$ - components of electric polarization in the presence of  $xy$ - and  $zx$ -plane spin spiral order respectively in symmetric M-O<sub>2</sub>-M chains (see Fig.7). A typical set of parameters are chosen for Cu<sup>2+</sup> oxides<sup>42</sup>,  $t_{pd\pi} = 0.75 \text{ eV}$ ,  $t_{pd\sigma} = -1.85 \text{ eV}$ ,  $\Delta = 3 \text{ eV}$ . The Clementi-Raimondi effective charges  $Z_{\text{O}}^{\text{eff}} = 4.45$  and  $Z_{\text{Cu}}^{\text{eff}} = 13.2$  are used for O<sup>2-</sup> and Cu<sup>2+</sup> ions respectively<sup>43</sup> and  $R_{\text{Cu-O}} = 1.445 \text{ \AA}$  (i.e., LiCuVO<sub>4</sub><sup>44</sup>).

In Fig.9, we plot  $y$ - and  $z$ - components of electric polarization as functions of bond-bending angle  $\varphi$  in the presence of  $xy$ - and  $zx$ -plane spin spiral order respectively. One sees that the polarization is sensitive to the bond bending angle  $\varphi$  and is anisotropic. In realistic materials, the bond angles of Cu-O-Cu in LiCuVO<sub>4</sub>, LiCu<sub>2</sub>O<sub>2</sub>, and NaCu<sub>2</sub>O<sub>2</sub> are  $95^\circ$ <sup>27</sup>,  $94^\circ$ <sup>25</sup>, and  $92.9^\circ$ <sup>36,37</sup> respectively, corresponding to bond bending angles  $\varphi = 42.5^\circ, 43^\circ$ , and  $43.6^\circ$ , which are all close to  $\varphi = \pi/4$ . As shown in the Fig. 9, the electric polarization decreases and ultimately vanishes when  $\varphi$  approaches  $\pi/4$ . Indeed, experiments clearly indicated that the electric polarization in LiCuVO<sub>4</sub> is stronger than that of LiCu<sub>2</sub>O<sub>2</sub>. Moreover, the bond-bending angle  $\varphi$  in NaCu<sub>2</sub>O<sub>2</sub> is closer to  $\pi/4$  than that of LiCuVO<sub>4</sub> and LiCu<sub>2</sub>O<sub>2</sub>, resulting in weaker electric polarization which is difficult to be observed.

For comparison, we also list calculated electric po-



TABLE I. The  $a$ - and  $c$ - components of electric polarizations in  $\text{LiCuVO}_4$ ,  $\text{LiCu}_2\text{O}_2$  and  $\text{NaCu}_2\text{O}_2$  in the presence of  $ab$ - and  $bc$ -plane spin spiral orders. The values in parentheses correspond to experimental data.

Materials	$\varphi$	Polarization ( $\mu\text{C}/\text{m}^2$ )	
		$P_a(ab)$	$P_c(bc)$
$\text{LiCuVO}_4^{27,28}$	$42.5^\circ$	5.8 (43)	4.3 (10)
$\text{LiCu}_2\text{O}_2^{24,25}$	$43^\circ$	4.4 (8)	3.8 (4)
$\text{NaCu}_2\text{O}_2^{40}$	$43.6^\circ$	2.1 (? <sup>a</sup> )	0.8 (0)

<sup>a</sup>Currently no experimental data is available.

larizations for these three compounds in Table I using their concrete parameters. For example, the pitch angles for  $\text{LiCuVO}_4$ ,  $\text{LiCu}_2\text{O}_2$  and  $\text{NaCu}_2\text{O}_2$  are  $84.2^\circ$ <sup>27,28</sup>,  $62.6^\circ$ <sup>25</sup>, and  $81.7^\circ$ <sup>40</sup> respectively. Corresponding  $R_{\text{Cu-O}}$  ( $R_{\text{Cu-O}}$  is the distance of Cu-O bond along the Cu-Cu chain) are  $1.445\text{\AA}$ <sup>44</sup>,  $1.43\text{\AA}$ <sup>25</sup>, and  $1.465\text{\AA}$ <sup>40</sup> respectively. Other parameters are the same as those in Fig.9. The values in parentheses in Table I are experimental data. The decreasing electric polarization with  $\varphi$  approaching  $\pi/4$  is in agreement with experimental observation. For  $\text{NaCu}_2\text{O}_2$  compound in the presence of  $bc$ -plane spin spiral order<sup>36,38</sup>, we find that  $P_c$  is extremely weak and hard to detect<sup>40</sup>. To our knowledge, there is no experimental report on electric polarization in the presence of  $ab$ -plane spin spiral order, which may be tunable under external field. Our theory predict a finite electric polarization ( $\sim 2\mu\text{C}/\text{m}^2$ ) oriented along the  $a$ -axis in the presence of  $ab$ -plane spin spiral order. This prediction can be tested in future experiment for  $\text{NaCu}_2\text{O}_2$ . Thus, the effect of bond-distortion on the magnetic-driven polarization provides a clue to clarify the anisotropy of the electric polarization observed in  $\text{LiCuVO}_4$  and  $\text{LiCu}_2\text{O}_2$  and to elucidate the puzzle of non-multiferroicity in  $\text{NaCu}_2\text{O}_2$ .

## VI. CONCLUSION

In this paper, we study how the distortion of M-O-M bonds affect the lowest lying electronic states thereby the electric polarization in multiferroic magnets. We calculate relevant low lying electronic states and electric polarization for three-atom M-O-M clusters and four-atom M-O<sub>2</sub>-M clusters respectively. It turns out that the electric polarization contains two parts, spin-current polarization which can be written in terms of  $\vec{e}_{i,j} \times (\vec{e}_i \times \vec{e}_j)$  and lattice-mediated polarization which exists only when the M-O-M bond angle deviates away from  $180^\circ$ .

For three-atom M-O-M clusters, both the spin-current polarization and the lattice-mediated polarization are of the order of  $(V/\Delta)$  in single-hole situation. However, the spin-current polarization is of the order of  $(V/\Delta)^3$  while the lattice-mediated polarization is of the order of  $(V/\Delta)$  in double-hole situation. Thus, the electric polarization in double-hole situation can be much larger than that estimated by spin-current mechanism<sup>8</sup> when M-O-M bond

distortion is present. For four-atom M-O<sub>2</sub>-M clusters, lattice-mediated polarization vanishes due to symmetry and there exists only spin-current polarization which is of the order of  $(V/\Delta)$  in single-hole situation and of the order of  $(V/\Delta)^3$  in double-hole situation.

Then we study three kinds of chain models made of different clusters where magnetic moments are spiral ordered. Firstly, we study uniform bond-distortion chain models where all the bridge oxygen atoms deviate from the spin chain formed by transition metal atoms in the same direction and with the same bond-bending angle. Ferroelectric order may exist in such chains. Secondly, we study staggered bending M-O-M chains in which the bridge oxygen atoms displace on opposite directions between two adjacent clusters. Ferrielectric order may appear instead of ferroelectric order in this kind of chains. Thirdly, we study symmetric M-O<sub>2</sub>-M chains which are made of four-atom M-O<sub>2</sub>-M clusters and the two oxygen atoms deviate symmetrically from the M-M bond within a M-O<sub>2</sub>-M cluster. The electric polarization may be ferroelectric ordered in such symmetric chains.

We also discuss the relation between magnetic-driven electric polarization and lattice-driven electric polarization in the presence of bond distortion in details.

Finally, we apply our theory to multiferroics copper oxides and find the results agree with experimental observations. The issue of “missing multiferroicity” in  $\text{NaCu}_2\text{O}_2$  compound is clarified and more experimental predictions are made.

Summarizing, we show that the M-O-M bond distortion may affect electric polarization in multiferroics significantly and the possibilities for ferroelectric and ferrielectric ordering are discussed. The application to multiferroics copper oxides is successful.

## ACKNOWLEDGEMENTS

This work is supported by National Basic Research Program of China(973 Program, No.2011CBA00103), NSFC(Grant No.11074216, 10874149 and 11074218), RFDP(No.20100101120002), PCSIRT(No.IRT0754), Doctoral Fund of Ministry of Education of China, and the Fundamental Research Funds for the Central Universities in China.

### Appendix A: Coefficients $A_{(j)}^{i\sigma}$ and $B_{(j)}^{i\sigma}$ in Eqs.(5)

In this appendix we shall derive coefficients  $A_{(j)}^{i\sigma}$  and  $B_{(j)}^{i\sigma}$  in Eqs.(5a) and (5b). For the parallel state  $|P_j\rangle$  and corresponding coefficients  $A_{(j)}^{i\sigma}$ , we combine Eqs.(4a) and (5a) to have

$$\sin \frac{\theta_j}{2} |a\rangle + e^{i\phi_j} \cos \frac{\theta_j}{2} |b\rangle = \sum_{i\sigma} A_{(j)}^{i\sigma} |d_{i\sigma}^{(j)}\rangle. \quad (\text{A1})$$

Using the relation Eq.(2), we obtain  $A_{(j)}^{i\sigma}$  as follows,

$$A_{(j)}^{xy,\uparrow} = \frac{1}{\sqrt{3}} \sin \frac{\theta_j}{2}, \quad (\text{A2a})$$

$$A_{(j)}^{xy,\downarrow} = \frac{1}{\sqrt{3}} e^{i\phi_j} \cos \frac{\theta_j}{2}, \quad (\text{A2b})$$

$$A_{(j)}^{yz,\uparrow} = -\frac{1}{\sqrt{3}} e^{i\phi_j} \cos \frac{\theta_j}{2}, \quad (\text{A2c})$$

$$A_{(j)}^{yz,\downarrow} = \frac{1}{\sqrt{3}} \sin \frac{\theta_j}{2}, \quad (\text{A2d})$$

$$A_{(j)}^{zx,\uparrow} = \frac{1}{\sqrt{3}} i e^{i\phi_j} \cos \frac{\theta_j}{2}, \quad (\text{A2e})$$

$$A_{(j)}^{zx,\downarrow} = \frac{1}{\sqrt{3}} i \sin \frac{\theta_j}{2}. \quad (\text{A2f})$$

Similarly, we obtain coefficients  $B_{(j)}^{i\sigma}$  for the anti-parallel state  $|AP_j\rangle$  as follows,

$$B_{(j)}^{xy,\uparrow} = \frac{1}{\sqrt{3}} \cos \frac{\theta_j}{2}, \quad (\text{A3a})$$

$$B_{(j)}^{xy,\downarrow} = -\frac{1}{\sqrt{3}} e^{i\phi_j} \sin \frac{\theta_j}{2}, \quad (\text{A3b})$$

$$B_{(j)}^{yz,\uparrow} = \frac{1}{\sqrt{3}} e^{i\phi_j} \sin \frac{\theta_j}{2}, \quad (\text{A3c})$$

$$B_{(j)}^{yz,\downarrow} = \frac{1}{\sqrt{3}} \cos \frac{\theta_j}{2}, \quad (\text{A3d})$$

$$B_{(j)}^{zx,\uparrow} = -\frac{1}{\sqrt{3}} i e^{i\phi_j} \sin \frac{\theta_j}{2}, \quad (\text{A3e})$$

$$B_{(j)}^{zx,\downarrow} = \frac{1}{\sqrt{3}} i \cos \frac{\theta_j}{2}. \quad (\text{A3f})$$

## Appendix B: Lowest lying eigenstates for three-atom M-O-M cluster

We calculate the eigenvectors for two lowest lying eigenstates  $|1\rangle$  and  $|2\rangle$  in a three-atom M-O-M cluster in this appendix. The Hilbert space contains states  $|P_j\rangle$ , ( $j = 1, 2$ ) and  $p_{\mu,\sigma}$  ( $\mu = x, y, z$ ,  $\sigma = \uparrow, \downarrow$ ). Assuming  $V \ll \Delta$  and treating  $H_t$  as a perturbation to  $H_\Delta$ , we obtain the two eigenvectors  $|1\rangle$  and  $|2\rangle$  up to the second order perturbation,

$$\begin{aligned} |1\rangle = & -\frac{B}{\sqrt{2}|B|} \left[ |P_1\rangle - \frac{1}{\Delta} \sum_{\sigma} \left( A_{(1)}^{xy,\sigma} (V_1 |p_{x,\sigma}\rangle + V_2 |p_{y,\sigma}\rangle) + (V_3 A_{(1)}^{zx,\sigma} + V_4 A_{(1)}^{yz,\sigma}) |p_{z,\sigma}\rangle \right) \right] \\ & + \frac{1}{\sqrt{2}} \left[ |P_2\rangle - \frac{1}{\Delta} \sum_{\sigma} \left( A_{(2)}^{xy,\sigma} (V_1 |p_{x,\sigma}\rangle - V_2 |p_{y,\sigma}\rangle) + (-V_3 A_{(2)}^{zx,\sigma} + V_4 A_{(2)}^{yz,\sigma}) |p_{z,\sigma}\rangle \right) \right], \end{aligned} \quad (\text{B1})$$

with  $E_1 = 2(C - |B|)$ , and

$$\begin{aligned} |2\rangle = & \frac{B}{\sqrt{2}|B|} \left[ |P_1\rangle - \frac{1}{\Delta} \sum_{\sigma} \left( A_{(1)}^{xy,\sigma} (V_1 |p_{x,\sigma}\rangle + V_2 |p_{y,\sigma}\rangle) + (V_3 A_{(1)}^{zx,\sigma} + V_4 A_{(1)}^{yz,\sigma}) |p_{z,\sigma}\rangle \right) \right] \\ & + \frac{1}{\sqrt{2}} \left[ |P_2\rangle - \frac{1}{\Delta} \sum_{\sigma} \left( A_{(2)}^{xy,\sigma} (V_1 |p_{x,\sigma}\rangle - V_2 |p_{y,\sigma}\rangle) + (-V_3 A_{(2)}^{zx,\sigma} + V_4 A_{(2)}^{yz,\sigma}) |p_{z,\sigma}\rangle \right) \right], \end{aligned} \quad (\text{B2})$$

with  $E_2 = 2(C + |B|)$ , where parameters  $C$  and  $B$  are given in Eqs. (12), (13) and (14) in the main text, coefficients  $A_{(j)}^{i\sigma}$  are given in Eqs.(A2). It is easy to verify that the states  $|1\rangle$  and  $|2\rangle$  are orthogonal to each other and their normalization factors are  $\langle 1|1\rangle = 1 - (C - |B|)/\Delta$  and  $\langle 2|2\rangle = 1 - (C + |B|)/\Delta$  respectively.

## Appendix C: Lowest lying eigenstates for four-atom M-O<sub>2</sub>-M cluster

In this appendix, we calculate the eigenvectors for two lowest lying eigenstates  $|1\rangle$  and  $|2\rangle$  in a four-atom M-O<sub>2</sub>-M cluster. In this situation, the Hilbert space contains

states  $|P_j\rangle$  ( $j = 1, 2$ ) and  $p_{\mu,\sigma}^{(i)}$  ( $i = 1, 2$ ,  $\mu = x, y, z$ ,  $\sigma = \uparrow, \downarrow$ ). Up to the second order of  $\frac{V}{\Delta}$ , we obtain the two

eigenvectors  $|1\rangle$  and  $|2\rangle$  as follows,

$$\begin{aligned} |1\rangle = & -\frac{A_1\alpha}{\sqrt{2}|A_1\alpha|} \left[ |P_1\rangle - \frac{1}{\Delta} \sum_{\sigma} \left( A_{(1)}^{xy,\sigma} \left( V_1 |p_{x,\sigma}^{(1)}\rangle + V_2 |p_{y,\sigma}^{(1)}\rangle \right) + \left( V_3 A_{(1)}^{zx,\sigma} + V_4 A_{(1)}^{yz,\sigma} \right) |p_{z,\sigma}^{(1)}\rangle \right. \right. \\ & \left. \left. - A_{(1)}^{xy,\sigma} \left( V_1 |p_{x,\sigma}^{(2)}\rangle - V_2 |p_{y,\sigma}^{(2)}\rangle \right) + \left( V_3 A_{(1)}^{zx,\sigma} - V_4 A_{(1)}^{yz,\sigma} \right) |p_{z,\sigma}^{(2)}\rangle \right) \right] \\ & + \frac{1}{\sqrt{2}} \left[ |P_2\rangle - \frac{1}{\Delta} \sum_{\sigma} \left( A_{(2)}^{xy,\sigma} \left( V_1 |p_{x,\sigma}^{(1)}\rangle - V_2 |p_{y,\sigma}^{(1)}\rangle \right) + \left( -V_3 A_{(2)}^{zx,\sigma} + V_4 A_{(2)}^{yz,\sigma} \right) |p_{z,\sigma}^{(1)}\rangle \right. \right. \\ & \left. \left. - A_{(2)}^{xy,\sigma} \left( V_1 |p_{x,\sigma}^{(2)}\rangle + V_2 |p_{y,\sigma}^{(2)}\rangle \right) + \left( -V_3 A_{(2)}^{zx,\sigma} - V_4 A_{(2)}^{yz,\sigma} \right) |p_{z,\sigma}^{(2)}\rangle \right) \right], \end{aligned} \quad (C1)$$

with  $E_1 = 2(C - |A_1\alpha|)$ , and

$$\begin{aligned} |2\rangle = & \frac{A_1\alpha}{\sqrt{2}|A_1\alpha|} \left[ |P_1\rangle - \frac{1}{\Delta} \sum_{\sigma} \left( A_{(1)}^{xy,\sigma} \left( V_1 |p_{x,\sigma}^{(1)}\rangle + V_2 |p_{y,\sigma}^{(1)}\rangle \right) + \left( V_3 A_{(1)}^{zx,\sigma} + V_4 A_{(1)}^{yz,\sigma} \right) |p_{z,\sigma}^{(1)}\rangle \right. \right. \\ & \left. \left. - A_{(1)}^{xy,\sigma} \left( V_1 |p_{x,\sigma}^{(2)}\rangle - V_2 |p_{y,\sigma}^{(2)}\rangle \right) + \left( V_3 A_{(1)}^{zx,\sigma} - V_4 A_{(1)}^{yz,\sigma} \right) |p_{z,\sigma}^{(2)}\rangle \right) \right] \\ & + \frac{1}{\sqrt{2}} \left[ |P_2\rangle - \frac{1}{\Delta} \sum_{\sigma} \left( A_{(2)}^{xy,\sigma} \left( V_1 |p_{x,\sigma}^{(1)}\rangle - V_2 |p_{y,\sigma}^{(1)}\rangle \right) + \left( -V_3 A_{(2)}^{zx,\sigma} + V_4 A_{(2)}^{yz,\sigma} \right) |p_{z,\sigma}^{(1)}\rangle \right. \right. \\ & \left. \left. - A_{(2)}^{xy,\sigma} \left( V_1 |p_{x,\sigma}^{(2)}\rangle + V_2 |p_{y,\sigma}^{(2)}\rangle \right) + \left( -V_3 A_{(2)}^{zx,\sigma} - V_4 A_{(2)}^{yz,\sigma} \right) |p_{z,\sigma}^{(2)}\rangle \right) \right], \end{aligned} \quad (C2)$$

with  $E_2 = 2(C + |A_1\alpha|)$ , where parameters  $C$ ,  $A_1$  and  $\alpha$  are given in Eqs. (12), (13) and (14) in the main text, coefficients  $A_{(j)}^{i\sigma}$  are given in Eqs.(A2). The normalization factors are  $\langle 1|1\rangle = 1 - 2(C - |A_1\alpha|)/\Delta$  and  $\langle 2|2\rangle = 1 - 2(C + |A_1\alpha|)/\Delta$ .

for nonvanishing  $I_{\mu,\nu}^{\alpha}(\vec{a})$ .

#### Appendix D: Overlap dipole matrix elements $I_{\mu,\nu}^{\alpha}(\vec{a})$

From the definition of the overlap dipole matrix elements  $I_{\mu,\nu}^{\alpha}(\vec{a})$  in Eq.(20), and using the mirror symmetry about the  $xy$ -plane ( $z \rightarrow -z$ ), we find that the following matrix elements vanish,

$$\begin{aligned} I_{xy,z}^x &= I_{yz,x}^x = I_{yz,y}^x = I_{zx,x}^x = I_{zx,y}^x = 0, \\ I_{xy,z}^y &= I_{yz,x}^y = I_{yz,y}^y = I_{zx,x}^y = I_{zx,y}^y = 0, \\ I_{xy,x}^z &= I_{yz,y}^z = I_{yz,z}^z = I_{zx,z}^z = 0. \end{aligned}$$

Then we study symmetry relations for nonvanishing  $I_{\mu,\nu}^{\alpha}(\vec{a})$  with two vectors  $\vec{a}$  and  $\vec{b}$ , where  $\vec{a}$  and  $\vec{b}$  lie within the  $xy$ -plane and are linked by symmetry  $P_x(x \rightarrow -x)$  or  $P_y(y \rightarrow -y)$ . When  $\vec{b} = P_x\vec{a}$  or  $\vec{b} = P_y\vec{a}$ , we have

$$\begin{aligned} I_{xy,y}^x(\vec{a}) &= I_{xy,y}^x(\vec{b}), I_{xy,x}^x(\vec{a}) = -I_{xy,x}^x(\vec{b}), \\ I_{yz,z}^x(\vec{a}) &= -I_{yz,z}^x(\vec{b}), I_{zx,z}^x(\vec{a}) = I_{zx,z}^x(\vec{b}), \\ I_{xy,x}^y(\vec{a}) &= I_{xy,x}^y(\vec{b}), I_{xy,y}^y(\vec{a}) = -I_{xy,y}^y(\vec{b}), \\ I_{yz,z}^y(\vec{a}) &= I_{yz,z}^y(\vec{b}), I_{yz,x}^y(\vec{a}) = -I_{yz,x}^y(\vec{b}), \\ I_{xy,z}^z(\vec{a}) &= -I_{xy,z}^z(\vec{b}), I_{yz,x}^z(\vec{a}) = -I_{yz,x}^z(\vec{b}), \\ I_{yz,y}^z(\vec{a}) &= I_{yz,y}^z(\vec{b}), I_{zx,x}^z(\vec{a}) = I_{zx,x}^z(\vec{b}), \\ I_{zx,y}^z(\vec{a}) &= -I_{zx,y}^z(\vec{b}), \end{aligned}$$

It turns out that relevant  $I_{\mu,\nu}^{\alpha}(\vec{a})$ 's in the main text include  $I_{yz,y}^z$ ,  $I_{xy,z}^z$ ,  $I_{yz,x}^z$ ,  $I_{xy,x}^y$ ,  $I_{yz,z}^y$ ,  $I_{zx,z}^y$ ,  $I_{xy,y}^y$ . We demonstrate the numerical evaluation for these integrals in Fig.10 and Fig.11 respectively.  $R_{M-O}$  is the M-O bond distance along the M-M chain. In this calculation, we have taken the hydrogenlike radial-wave functions and the Clementi-Raimondi effective charges  $Z_O^{\text{eff}} = 4.45$  and  $Z_M^{\text{eff}} = 10.53$  for  $O^{2-}$  and  $Mn^{3+}$  ions respectively<sup>43</sup>. It is shown that, for typical M-O separation (i.e.,  $R_{M-O} \sim 4a_0$ , here  $a_0$  is Bohr radius),  $I_{xy,x}^y$  is one order of magnitude larger than those of other integrals. The separation between the M and O ions  $R_{M-O}$  not only yields violent variance on the magnitude of the overlap dipole integrals but also may change their signs.

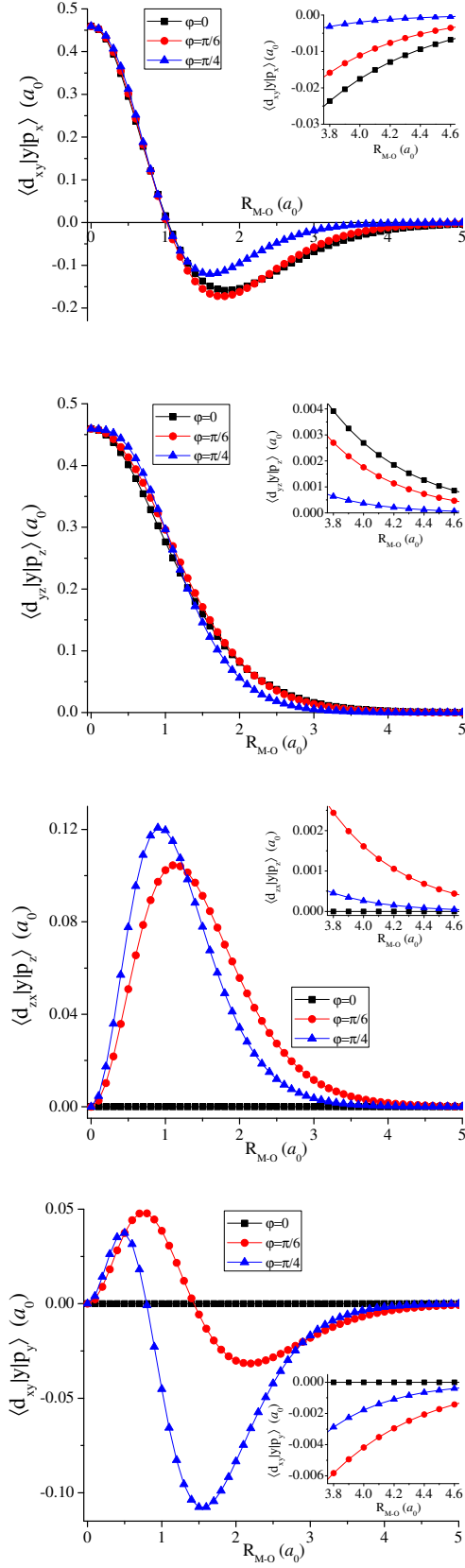


FIG. 10. Two-site dipole integrals  $I_{\mu,\nu}^y$  against M-O separation  $R_{M-O}$  with various bond bending angle. The inset in each figure shows the zoom in view of the integrals near typical M-O separation (i.e.,  $4a_0$ ,  $a_0$  is the Bohr radius).

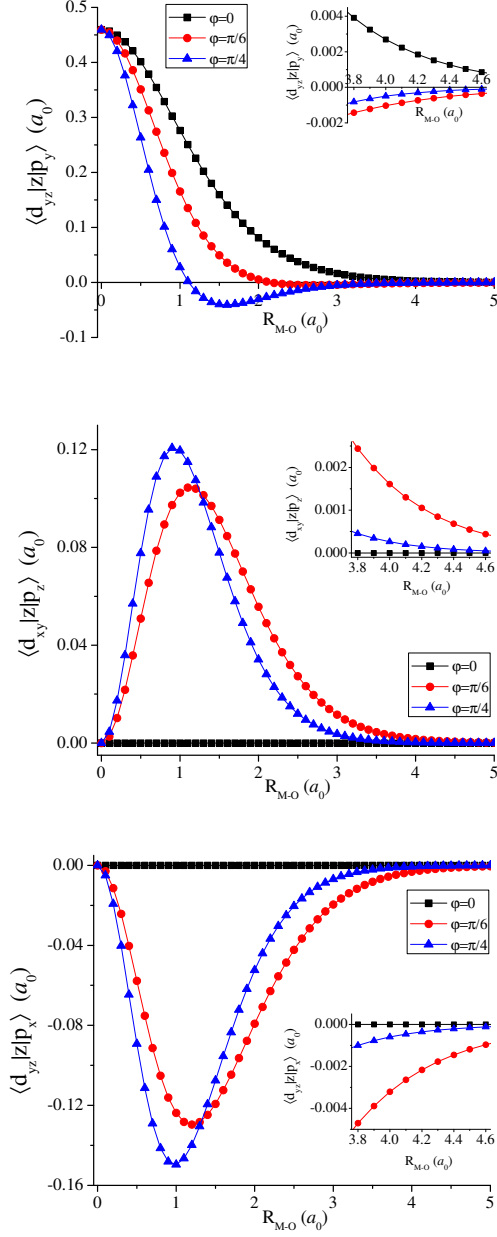


FIG. 11. Two-site dipole integrals  $I_{\mu,\nu}^z$  against M-O separation  $R_{M-O}$  with various bond bending angle. The inset in each figure shows the zoom in view of the integrals near typical M-O separation (i.e.,  $4a_0$ ).

<sup>1</sup> M. Fiebig, J. Phys. D **38**, R123 (2005).

<sup>2</sup> N. A. Hill, J. Phys. Chem. B **104**, 6694 (2000).

<sup>3</sup> T. Kimura, T. Goto, H. Shintani, K. Ishizaka, T. Arima, and Y. Tokura, Nature (London) **426**, 55 (2003).

<sup>4</sup> M. Kenzelmann, A. B. Harris, S. Jonas, C. Broholm, J. Schefer, S. B. Kim, C. L. Zhang, S.-W. Cheong, O. P. Vajk, and J. W. Lynn, Phys. Rev. Lett. **95**, 087206 (2005).

<sup>5</sup> S.-W. Cheong and M. Mostovoy, Nature Mater. **6**, 13

(2007).

<sup>6</sup> D. Khomskii, Physics **2**, 20 (2009).

<sup>7</sup> K. F. Wang, J.-M. Liu, and Z. F. Ren, Adv. Phys. **58**, 321 (2009).

<sup>8</sup> H. Katsura, N. Nagaosa, and A. V. Balatsky, Phys. Rev. Lett. **95**, 057205 (2005).

<sup>9</sup> C. Jia, S. Onoda, N. Nagaosa, and J. H. Han, Phys. Rev. B **74**, 224444 (2006).

- <sup>10</sup> C. Jia, S. Onoda, N. Nagaosa, and J. H. Han, Phys. Rev. B **76**, 144424 (2007).
- <sup>11</sup> J. Hu, Phys. Rev. Lett. **100**, 077202 (2008).
- <sup>12</sup> C. D. Hu, Phys. Rev. B **75**, 172106 (2007).
- <sup>13</sup> C. D. Hu, Phys. Rev. B **77**, 174418 (2008).
- <sup>14</sup> C. D. Hu, Phys. Rev. B **81**, 224414 (2010).
- <sup>15</sup> I. A. Sergienko and E. Dagotto, Phys. Rev. B **73**, 094434 (2006).
- <sup>16</sup> M. Mochizuki, N. Furukawa, and N. Nagaosa, Phys. Rev. Lett. **105**, 037205 (2010).
- <sup>17</sup> M. Mochizuki, N. Furukawa, and N. Nagaosa, Phys. Rev. B **84**, 144409 (2011).
- <sup>18</sup> M. Mostovoy, Phys. Rev. Lett. **96**, 067601 (2006).
- <sup>19</sup> Y. Yamasaki, H. Sagayama, T. Goto, M. Matsuura, K. Hirota, T. Arima, and Y. Tokura, Phys. Rev. Lett. **98**, 147204 (2007).
- <sup>20</sup> T. Goto, T. Kimura, G. Lawes, A. P. Ramirez, and Y. Tokura, Phys. Rev. Lett. **92**, 257201 (2004).
- <sup>21</sup> K. Taniguchi, N. Abe, T. Takenobu, Y. Iwasa, and T. Arima, Phys. Rev. Lett. **97**, 097203 (2006).
- <sup>22</sup> G. Lawes, A. B. Harris, T. Kimura, N. Rogado, R. J. Cava, A. Aharony, O. Entin-Wohlman, T. Yildirim, M. Kenzelmann, C. Broholm, and A. P. Ramirez, Phys. Rev. Lett. **95**, 087205 (2005).
- <sup>23</sup> Y. Yamasaki, S. Miyasaka, Y. Kaneko, J.-P. He, T. Arima, and Y. Tokura, Phys. Rev. Lett. **96**, 207204 (2006).
- <sup>24</sup> S. Park, Y. J. Choi, C. L. Zhang, and S.-W. Cheong, Phys. Rev. Lett. **98**, 057601 (2007).
- <sup>25</sup> S. Seki, Y. Yamasaki, M. Soda, M. Matsuura, K. Hirota, and Y. Tokura, Phys. Rev. Lett. **100**, 127201 (2008).
- <sup>26</sup> Y. Naito, K. Sato, Y. Yasui, Y. Kobayashi, Y. Kobayashi, and M. Sato, J. Phys. Soc. Jpn. **76**, 023708 (2007).
- <sup>27</sup> Y. Yasui, Y. Naito, K. Sato, T. Moyoshi, M. Sato, and K. Kakurai, J. Phys. Soc. Jpn. **77**, 023712 (2008).
- <sup>28</sup> F. Schrettle, S. Krohns, P. Lunkenheimer, J. Hemberger, N. Bütgen, H.-A. Krug von Nidda, A. V. Prokofiev, and A. Loidl, Phys. Rev. B **77**, 144101 (2008).
- <sup>29</sup> M. Mourigal, M. Enderle, R. K. Kremer, J. M. Law, and B. Fåk, Phys. Rev. B **83**, 100409(R) (2011).
- <sup>30</sup> T. Kimura, S. Ishihara, H. Shintani, T. Arima, K. T. Takahashi, K. Ishizaka, and Y. Tokura, Phys. Rev. B **68**, 060403(R) (2003).
- <sup>31</sup> T. Arima, A. Tokunaga, T. Goto, H. Kimura, Y. Noda, and Y. Tokura, Phys. Rev. Lett. **96**, 097202 (2006).
- <sup>32</sup> A. S. Moskvina and S.-L. Drechsler, Phys. Rev. B **78**, 024102 (2008).
- <sup>33</sup> J. C. Slater and G. F. Koster, Phys. Rev. **94**, 1498 (1954).
- <sup>34</sup> L. D. Landau and E. M. Lifshitz, Quantum Mechanics (Pergamon Press Ltd., London, 1991), Sec. 39, p138.
- <sup>35</sup> T. Mizokawa and A. Fujimori, Phys. Rev. B **51**, 12880(R) (1995).
- <sup>36</sup> L. Capogna, M. Mayr, P. Horsch, M. Raichle, R. K. Kremer, M. Sofin, A. Maljuk, M. Jansen, and B. Keimer, Phys. Rev. B **71**, 140402(R) (2005).
- <sup>37</sup> K.-Y. Choi, V. P. Gnezdilov, P. Lemmens, L. Capogna, M. R. Johnson, M. Sofin, A. Maljuk, M. Jansen, and B. Keimer, Phys. Rev. B **73**, 094409 (2006).
- <sup>38</sup> A. A. Gippius, A. S. Moskvina, and S.-L. Drechsler, Phys. Rev. B **77**, 180403(R) (2008).
- <sup>39</sup> L. Capogna, M. Reehuis, A. Maljuk, R. K. Kremer, B. Ouladdiaf, M. Jansen, and B. Keimer, Phys. Rev. B **82**, 014407 (2010).
- <sup>40</sup> Ph. Leininger, M. Rahlenbeck, M. Raichle, B. Bohnenbuck, A. Maljuk, C. T. Lin, B. Keimer, E. Weschke, E. Schierle, S. Seki, Y. Tokura, and J. W. Freeland, Phys. Rev. B **81**, 085111 (2010).
- <sup>41</sup> H. J. Xiang and M.-H. Whangbo, Phys. Rev. Lett. **99**, 257203 (2007).
- <sup>42</sup> W. E. Pickett, Rev. Mod. Phys. **61**, 433 (1989).
- <sup>43</sup> E. Clementi and D. L. Raimondi, J. Chem. Phys. **38**, 2686 (1963).
- <sup>44</sup> H.-J. Koo, C. Lee, M.-H. Whangbo, G. J. McIntyre, and R. K. Kremer, Inorg. Chem. **50**, 3582 (2011).